Plasma Chemistry and Plasma Processing (2026) 46:57
https://doi.org/10.1007/s11090-026-10666-4

ORIGINAL PAPER

Investigation of Surface Morphology Evolution During the Borosilicate Glass Etching by Using ICP-RIE For Microfluidic Applications

Duygu Nuhoğlu[1,2] · Meryem Sarigüzel[2] · Cihat Taşaltın[2] · Ilke Gurol[2] · Esra Zayim[1]

Received: 22 October 2025 / Accepted: 14 April 2026 / Published online: 27 April 2026
© The Author(s) 2026

Abstract
Dry etching techniques are extensively used in the fabrication of silicon-based electronic components; however, the increasing use of glass substrates in microfluidic applications, due to their chemical stability, biocompatibility, optical transparency, electrical insulation, and cost-effectiveness, has created a growing demand for efficient dry etching of glass. This work presents the etching of borosilicate glasses using inductively coupled plasma reactive ion etching (ICP-RIE) with fluorine-based gas chemistries for use in microfluidic applications. Microfluidic structures were patterned via photolithography technic with micropillar were patterned using a titanium/gold stack and a nickel hard mask. The effects of various gas mixtures on the etch rate and surface morphology were systematically investigated. Optical emission spectroscopy (OES) was employed to monitor plasma characteristics, while surface analyses and etch depth were carried out using scanning electron microscopy (SEM), energy-dispersive X-ray spectroscopy (EDS), and profilometry, respectively. The results highlight how different gas compositions influence etch behavior and surface morphology, offering valuable insight for optimizing dry etching processes in glass-based microfluidic device fabrication and emphasize the importance of selecting appropriate gas ratios to achieve uniform microstructures with minimal surface defects.

Keywords Borofloat etching · Plasma etching · C_4F_8 plasma · Optical emission spectroscopy

Introduction

One of the most important steps in Micro-Electro-Mechanical System (MEMS) fabrication is the selection of substrate. Although silicon wafers remain of great importance in MEMS due to their crystalline structure and compatibility with established processes, glass substrates offer distinct advantages that make them increasingly attractive for advanced applications. The chemical and thermal stability of glass supports durability in aggressive

Extended author information available on the last page of the article

environments, and large-area availability provides scalability for applications such as lab-on-chip platforms. Furthermore, glass enhances biomedical performance in microfluidics owing to its inherent optical transparency, excellent electrical insulation, and biocompatibility, allowing for real-time examination. Within microfluidic systems, particle manipulation and separation can be achieved through specialized designs. For instance, deterministic lateral displacement (DLD) designs separate particles based on size, shape, and fluid flow, using microchannels filled with a regular array of micropillar obstacles [1]. The optical transparency of the glass further facilitates accurate detection of particle separation. Taken together, these properties highlight the clear advantages of glass as a MEMS substrate, enabling functionalities that extend beyond those offered by traditional substrates.

Another important step is etching, which is a critical step for high-resolution MEMS fabrication in hard materials, including silicon and glass [2]. Besides the advantages, etching of the glass is more complex than that of silicon due to its amorphous structure. Wet etching methods, such as those based on potassium hydroxide [3], provide limited capability for production high-aspect-ratio features, which are critical in many microfabrication applications. In contrast, dry etching enables directional etching and improved control over feature dimensions [4], but it requires careful optimization of plasma chemistry, process parameters, surface morphology, and masking materials for successful application. Even though dry etching processes have been predominantly developed and optimized based on silicon, their adaptation to glass poses distinct challenges, as glass remains relatively underexplored and demands further technological advancement.

Conventional Reactive Ion Etching (RIE) processes, one of the dry etching techniques, the substrate power and coil power are coupled to each other often resulting in etch non-uniformity across the substrate. However, in an Inductively Coupled Plasma (ICP) RIE system, the substrate power and the coil power are independent of each other. This feature allows outstanding regulation over plasma density (controlled by coil power), energy of etchant ions (controlled by substrate power) and generates stable plasma under low pressures necessary for removal of etching byproducts. The ICP RIE has separate power sources for the generation of radicals and ions (ICP – coil power) as plasma form and the acceleration of the ions (RF bias – substrate power), enabling them to etch a wide range of materials, including silicon, glass, and $LiNbO_3$, etc. During these processes, plasma is typically generated from fluorine-containing gases such as octafluorocyclobutane (C_4F_8) and sulfur hexafluoride (SF_6) [5]. The C_4F_8 gas dissociates in the plasma phase like CF_x to produce fluorocarbon species, which can deposit on the surface as Teflon-like polymer layers, providing sidewall protection during etching. Furthermore, the incorporation of Ar and O_2 serves to enhance physical sputtering and control surface polymerization, thereby improving the etching selectivity [6, 7]. In fluor-based plasma etching, maintaining a balance between ion-induced erosion and surface passivation is critical to achieve uniform etching. Excessive ion bombardment can cause sputter-effect-induced erosion, leading to surface roughness and material redeposition, while insufficient ion energy limits etch efficiency. A well-balanced condition enables steady etching by sustaining the interplay between sputter-effect-induced erosion and chemical reactions, ensuring uniform and reproducible surface morphology. The ICP RIE of especially on glass, contains a combination of physical ion bombardment by ions and chemical reactions driven by fluorine radicals. Since amorphous materials like borosilicate glass, composed mainly of boron, sodium, aluminum, and potassium oxides, exhibit strong chemical bonds and low sputter reveal, high-energy ions are required to initi-

ate material removal. Schematic illustration of plasma-assisted glass etching with ICP RIE is given in Fig. 1.

The application of RF bias power over plasma accelerates positively charged ions toward the substrate, enhancing anisotropic etching. Fluorine radicals react with substrate constituents to form volatile halogen compounds such as SiF_4 and BF_3, which are evacuated from the chamber, easily removed from the surface. However, stray particles, non-volatile halogen products like AlF_3, NaF, and KF which are physically sputtered from the surface [8], and incomplete reactions may also lead to surface contamination or etch profile irregularities. Failure to remove these non-volatile products can lead to coat the etching equipment or redeposit on the surface being etched by causing micro-masking and significantly reducing the etch rate [9]. Therefore, effective control of plasma parameters and gas composition is critical for achieving clean, anisotropic etch profiles in glass substrate.

To achieve precise and deep glass etching, the use of a sacrificial metal layer as a hard mask is vital, as it provides the necessary selectivity and structural integrity during the etching process. Chromium or nickel (Ni) thin films have been used as hard mask, because the polymeric thin films like photoresist has not enough selectivity to etch tens of microns of glass surface. Further, high aspect ratio devices requiring deep plateaus (> 10 µm) demand thick Ni hard masks for high-selectivity etching. E-beam evaporated Ni films exhibit significant strain and adhesion issues, particularly at thicknesses above 200 nm thickness, with resulting delamination from the device [10]. To address these challenges, electroplating provides a low-stress alternative, enabling thick, vertical Ni masks with sufficient selectivity for energetic ion etching, preserving surface integrity for further processing [10]. While the optimization of hard mask materials, such as electroplated Ni, is necessary to achieve high-selectivity and deep glass etching, another critical consideration lies in the surface-related challenges that can significantly influence etch performance and device reliability.

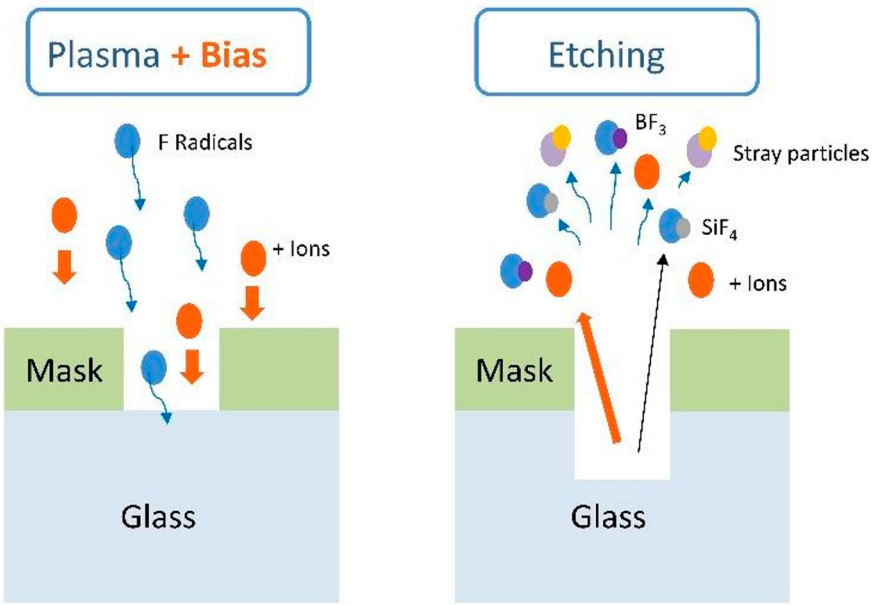

Fig. 1 Schematic illustration of plasma-assisted glass etching with ICP RIE

The surface damage can be categorized as; (a) deposited teflon-like fluorocarbon top passivation layer, (b) roughening of the substrate surface, (c) re-deposited of etched products like non-volatile substances (micro-masking), (d) lattice distortion due to sputter effect of etching. It was known that surface damages categorized as c) and d), called this phenomenon plasma-induced surface damage (PISD). PISD reduces the etch rate of glass since rough surface and micro-masking effect, also it is very difficult to remove these residues on a rough surface [11]. The etching process is a mixture between physical bombardment and chemical reaction, and the relationship between the increase of PISD formation and the dominance of physical etching has been established. Given the complexity of PISD and its impact on etch performance, in-situ diagnostic techniques become key insight into plasma–surface interactions. Among these, Optical Emission Spectroscopy (OES) has emerged as a widely used diagnostic tool for plasma-based etching processes due to its simplicity, non-intrusive nature, and capability for real-time monitoring [5]. The technique relies on detecting the spectrum of radiation emitted by excited species after energy absorption, known as the emission spectrum. By analyzing these emissions, OES provides valuable information into chamber conditions, plasma composition, and reaction byproducts formed at the surface. OES captures signals from plasma neutrals such as free radicals, which have lower excitation thresholds than ions, making it a powerful diagnostic tool for understanding and monitoring plasma-assisted etching processes [12].

In this work, borofloat glass substrates patterned with microfluidic column structures were etched using ICP-RIE with various SF_6, C_4F_8, Ar, and O_2 gas mixtures. Real-time OES was employed to monitor plasma species, while SEM, EDS, profilometry, and optical microscopy were used to analyze surface morphology, confirm PISD formation, and relate it to changes in surface morphology and etch rate. The aim of this study is to elucidate the relationship between plasma composition, etch behavior, and PISD formation, providing insights for the optimization of glass etching processes. The results show that gas chemistry strongly affects etch rate, surface morphology, and residue formation, revealing the mechanisms of PISD and its impact on glass processing. These insights provide practical guidelines for optimizing glass etching, enabling more reliable fabrication of microfluidic devices. It was found that the effective control of plasma gas composition was crucial for achieving clean, deep and stable etch profiles in glass substrates.

Materials and Methods

Experimental Setup

A microfluidic system pattern with micropillar-shaped obstacles was designed using Tanner Tools L-Edit software. The microfluidic structure is presented in Fig. 2, where the DLD microchannel was designed using three sequential segments of periodic cylindrical micropillar arrays with diameters of 30, 20, and 10 μm, respectively. This configuration, known as a cascade array [13], enables stepwise variation of the critical diameter along the flow path. Each array is tilted with respect to the main flow direction so that particles larger than the segment-specific critical diameter (Dc) are forced into the displacement mode, while smaller particles follow the streamlines. The progressive reduction in micropillar diameter and inter-post spacing produces a stepwise decrease in Dc along the channel, providing a

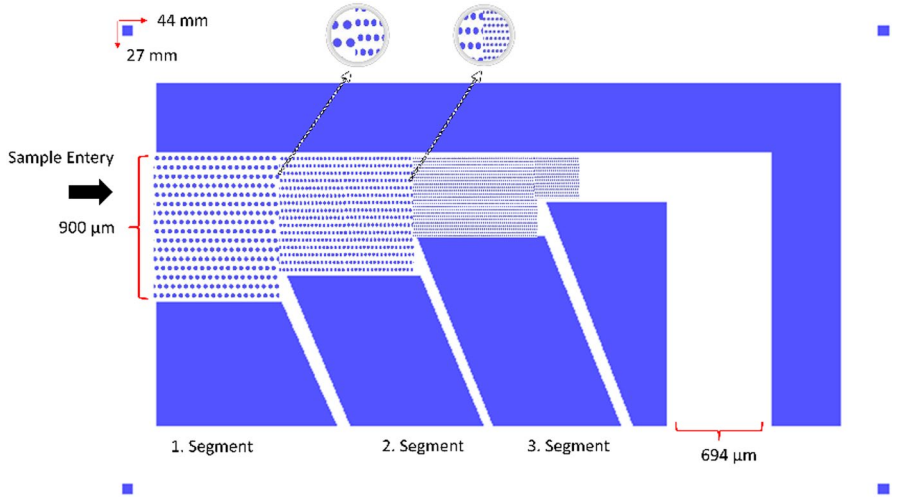

Fig. 2 Schematic illustration of microfluidic design

coarse-to-fine separation cascade that enhances resolution for progressively smaller particles as they travel downstream.

Borofloat33 glass glass substrates (0.7 cm thickness, composition 81% SiO_2, 13% B_2O_3, 2% Al_2O_3, 4% Na_2O/K_2O) were purchased from SCHOTT Glass, were patterned by photolithography using a high-resolution laser lithography system (DWL66 + by Heidelberg Instruments, with 10 mm write head mode). The positive tone and 3.3 µm thick Az4533 UV-sensitive photoresist (PR) was used, developed after exposing with Az400K developer, which was supplied from MicroChemicals. Metal layers were coated with the physical vapor deposition technique with the Nanovak NVEB-600 electron beam evaporation system. The sacrificial metal layers, such as titanium (Ti) and gold (Au), were wet etched with TiW etch 200 and TechniEtchTM ACl_2, respectively (MicroChemicals). Ni, which is used as a protective mask in etching materials such as glass, was coated with the electrodeposition technique, and the content of the bath used contains Ni sulphate ($NiSO_4.6H_2$), Ni chloride ($NiCl_2.6H_2O$) and boric acid (H_3BO_3) was purchased from SigmaAldrich [14].

Plasma etching was carried out by varying the process parameters such as gas chemistry, gas flow ratio, process pressure under by keeping the constant top and bottom electrode powers. An Oxford Cobra100 ICP-RIE system was used to etch a 10-20-30 µm diameter micropillar-shaped microfluidic pattern on glass substrate. Plasma generation was controlled by a 13.56 MHz top electrode power. Further, the bottom electrode power was supplied by a 4 MHz RF generator to induce the negative DC self-bias voltage. The substrate backside temperature of the wafer chuck during etching was held constant at 20 °C temperature by circulating the cooling ethylene glycol using a chiller. The etching chamber was evacuated using a large capacity turbo molecular pump during the process which makes it possible to reduce collision between reaction products and the surface of the substrate. Also, owing to this characteristic of the etcher, it is possible to etch materials like glass which produce nonvolatile reaction products. The oxygen cleaning protocol was performed between experiments to remove possible polymer deposition off the sidewalls of the plasma reactor chamber for 10 min, minimize contamination, and preserve repeatability from run to run.

Furthermore, OES was carried out to investigate the species present in plasma composition. A Verity Instrument (Model SD1024GH) spectrometer was used to record optical response from 300 nm to 800 nm with a low resolution (0.5 nm) every 0.5 s. Spectra View™ was used to post-process the collected data. The spectrometer was connected to the ICP RIE reactor chamber through an optical fiber cable attached to an external viewing port along the reactor wall. A schematic illustration of the system is given in Fig. 3.

After completing of ICP RIE process, the etching depths of the substrates were measured using a Bruker DektakXT stylus profilometer. The surface morphology was initially examined with an optical microscope, followed by detailed images of scanning electron microscopy (SEM) by using FEG 250 Field Emission. Elemental analyses, Energy Dispersive X-Ray Spectroscopy (EDS), of the island-like structures observed on the surface were conducted via JEOL JSM-6510 LV - Oxford Instruments INCA-EDS. The compositional accuracy for major elements is typically reported to be within approximately ± 2% relative uncertainty.

Sample Preparation

The detailed process flow of microfluidic fabrication on glass is shown in Fig. 4. Substrates were cleaned with Isopropyl Alcohol (IPA), acetone and, rinsed with deionized water respectively, then dried with nitrogen gas flow.

First, a stack of 50 nm Ti, 50 nm Au layers was deposited onto substrates, using electron beam evaporation (Fig. 4: a)). Subsequently, PR layer was deposited on the metal layer via spin-coating and structured with maskless photolithography to open windows for the fabrication of a microfluidic pattern (Fig. 4: b)). The PR application and exposure parameters are summarized in Table 1.

The Ti sub-layer coating ensured good adhesion between the glass and Au film, and Au film served as a seed layer for the electroplating of Ni for the next steps. The metal-coated and PR patterned glass substrates were used as the working electrode, Ni plate anode as a counter electrode into the Ni chloride-based electrodeposition bath under 10.25 mA current. The thickness of the Ni hard mask was kept at 4 µm for high selective etching and deposited on the PR patterned substrates (Fig. 4: c)). At the end of processes, the remaining PR was cleaned with acetone; Ti and, Au was removed by wet etching in areas outside of Ni (Fig. 4: d), e)), respectively. The blue region shown in Fig. 2 represents the area that will remain

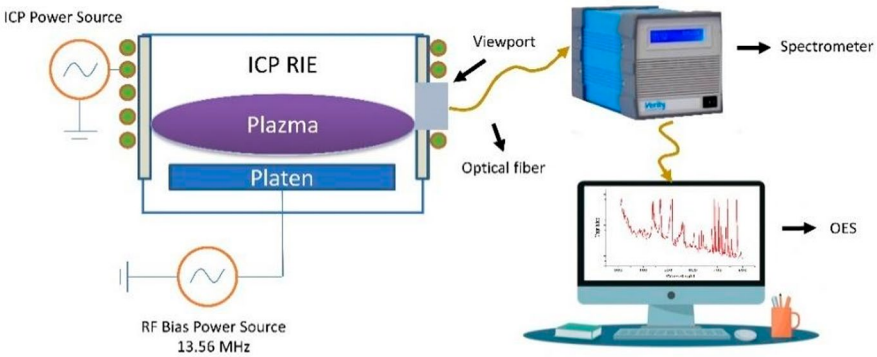

Fig. 3 Schematic illustration of the ICP RIE and spectrometer system

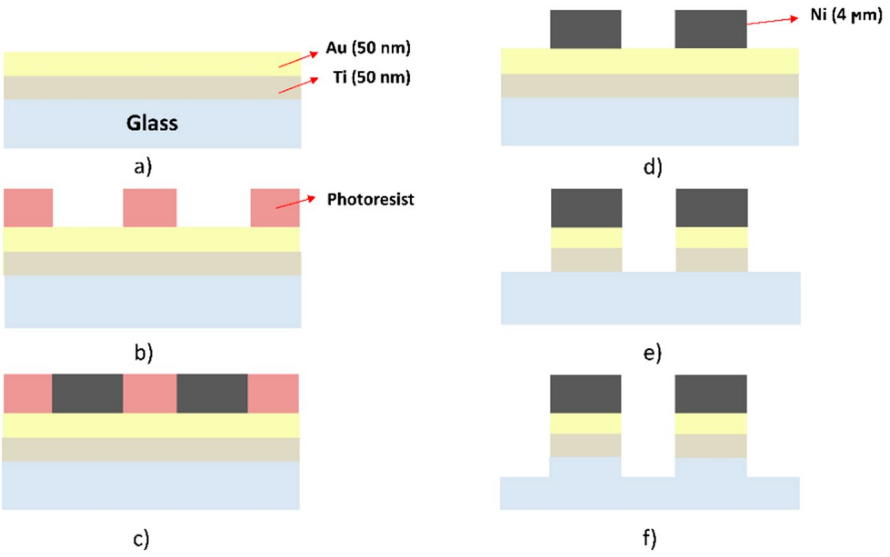

Fig. 4 Schematic illustration of sample preparation and etching. (**a**) Ti/Au multilayer deposition on cleaned borosilicate glass, (**b**) Photoresist coating and patterning, (**c**) Electrodeposition of Ni layer, (**d**) Remove photoresist by acetone, (**e**) Removing of sacrificial metal layers by etchant, (**f**) Etching of borosilicate glass using ICP-RIE of glass

Table 1 The PR application and exposure parameters

PR application parameters		Exposure parameters	
Dehydration	150 °C–1 min	Write head	10 mm
Hexamethyldisilane (HMDS) vapor treatment	40 seconds	Write laser	355 nm, Diod
		Laser Power	65 mW
Spin coating	3000 rpm – 1 min	Laser Intensity	80%
Prebake	100 °C –1 min		
	Exposure		
Develop	1:3 diluted Az400K – 1 min		

unetched. Hence, the final layers illustrated in Fig. 4: e) serve as a protective coating against ICP-RIE during the patterning of glass microstructures. The schematic representation of the desired microfluidic structure shown in Fig. 2, obtained after etching under different recipes, is presented in Fig. 4: f).

Figure 5 presents image of the prepared microfluidic structure on the borosilicate glass substrates, whose design and fabrication were completed, taken under laboratory conditions prior to the etching process.

The core objective of this study was to systematically investigate the influence of different plasma compositions on glass etching; therefore, the ICP-RIE chamber parameters summarized in Table 2 were employed to develop and compare four distinct gas mixtures, designated as Recipes A, B, C, and D. ICP power at 2000 W, table temperature (chuck temperature) at 20 °C, helium "back-side" pressure at 1.33 Pa, and RF bias power at 300 W was kept constant to eliminate any other variables. The experimental study began with Recipe A, which was optimized to establish the baseline etching conditions. To examine the combined

Fig. 5 Image of the prepared microfluidic structure

Table 2 ICP RIE process parameters for glass etching

ID	Gas flow rates (sccm)				RF bias (W)	ICP Power (W)	Pressure (Pa)
	SF_6	C_4F_8	Ar	O_2			
A	8	-	50	-	300	2000	0.667 (5 mTorr)
B	8	5	50	50	300	2000	0.667 (5 mTorr)
C	8	25	50	50	300	2000	0.667 (5 mTorr)
D	-	40	-	20	300	2000	1.33 (10 mTorr)

effect of C_4F_8 and O_2, Recipe B was then introduced. Subsequently, Recipe C was designed by further increasing the C_4F_8 flow rate in order to isolate its influence.

As shown in Table 2, in Recipes A–C, all contain Ar gas, which contributes to plasma formation, while in Recipe D, the removal of Ar resulted in unstable discharge at 5 mTorr. Argon, as an inert noble gas, possesses abundant metastable states that enhance electron-impact ionization and facilitate plasma ignition even under low-pressure conditions. The presence of Ar ensures a high density of energetic metastable atoms, which play a crucial role in sustaining the discharge through stepwise ionization and secondary electron emission at the cathode [15], thereby lowering the effective breakdown voltage and stabilizing the plasma at reduced pressures. In contrast, oxygen is an electronegative gas: it readily captures free electrons to form negative ions, which reduces the population of free electrons available to sustain the avalanche ionization. This electron loss increases the effective breakdown voltage and reduces plasma stability at low pressures [16]. Consequently, in Recipe D, the absence of Ar metastables and the electron attachment behavior of O_2 resulted in insufficient plasma generation at 5 mTorr. To overcome this, the chamber pressure was raised to 10 mTorr to reduce the required breakdown voltage and enable stable plasma ignition. Hence, the removal of argon from the recipes was intended to deliberately reduce ion bombardment and thereby minimize the PISD formation.

Results and Discussion

Surface Morphology and Compositional Analysis

Optical microscope images of the glass surfaces etched for 60 min with different plasma recipes were captured at a magnification of 20x and are presented in Fig. 5. The images show that plasma interaction significantly damages the surface, with the damage's extent and shape varying with the gas compositions.

In Recipe A (SF_6 + Ar), the presence of Ar promotes a sputter-effect-like process, which causes PISD, Fig. 6: a). When O_2 and C_4F_8 were added to the initial recipe to form Recipe B (SF_6 + Ar+O_2 + low C_4F_8), dark, scattered crater-like features were observed, as shown in Fig. 6: b). Using Recipe C (SF_6 + Ar+O_2 + high C_4F_8), in which the amount of C_4F_8 is increased, the microscope images revealed a more densely populated with overlapping structures Fig. 6: c). In particular, dark and scattered spot regions suggest particle redeposition effects, whereas under conditions such as Recipe D (O_2+higher C_4F_8) (Fig. 6: d), the

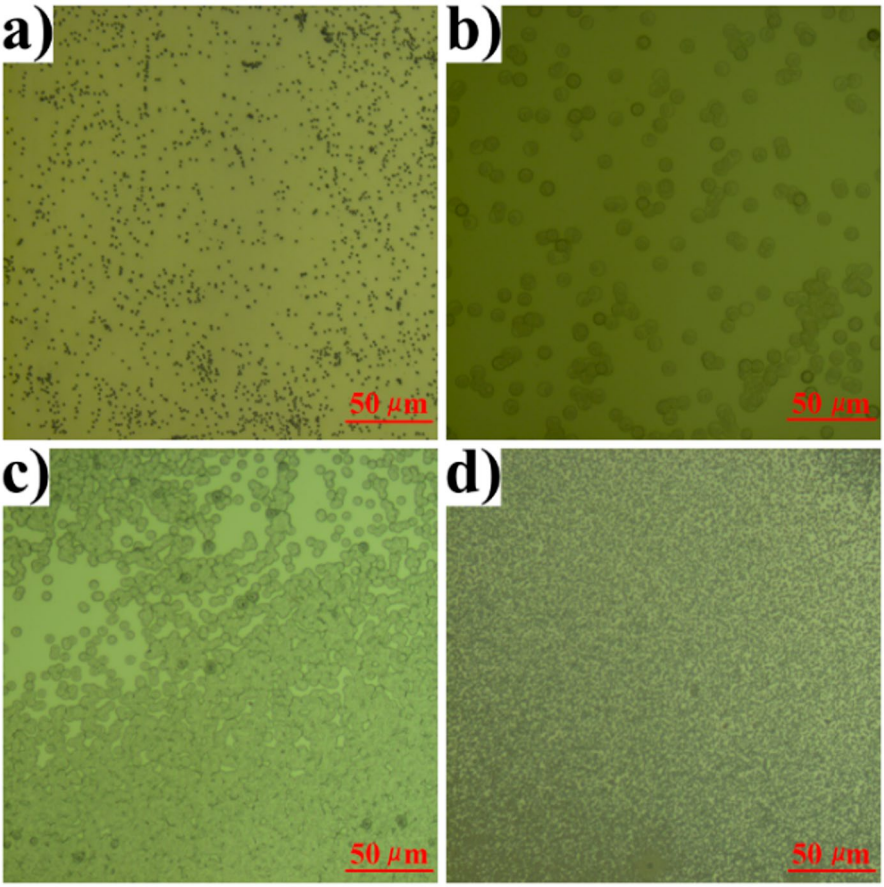

Fig. 6 Optical microscope images of the glass surfaces after 60 min of etching with Recipe (**a)** A, (**b)** B, (**c)** C, (**d)** D

surface appears more uniformly modified with reduced large-scale defect formation. These observations suggest that the plasma–surface interaction, including ion bombardment, chemical etching, and redeposition phenomena, strongly depends on the process chemistry, with specific gas composition significantly influencing PISD formation.

SEM images of the glass surface after 60 min with different plasma recipes are shown in Fig. 7. Spherical to irregular particle-like agglomerates scattered across the surface were observed in Fig. 7: a). This feature suggests redeposition of the etched material caused by sputter-effect-induced erosion. Such behavior is attributed to the sputter dominant etching regime due to high Ar concentration in Recipe A. Unlike Recipe A, where the high Ar content induced strong sputter-effect-induced erosion accompanied material redeposition, the addition of C_4F_8 and O_2, forming Recipe B, fundamentally altered the plasma chemistry and led to a marked suppression of the etching process. In Fig. 7: b), crater-like features observed in optical microscopy (Fig. 6: b)) were also confirmed by SEM analysis. The surface morphology was characterized by sparsely distributed, circular features surrounded by relatively smooth regions. In addition, bright residual islands were observed on the surface. These high-contrast regions were attributed to locally retained residues or redeposited

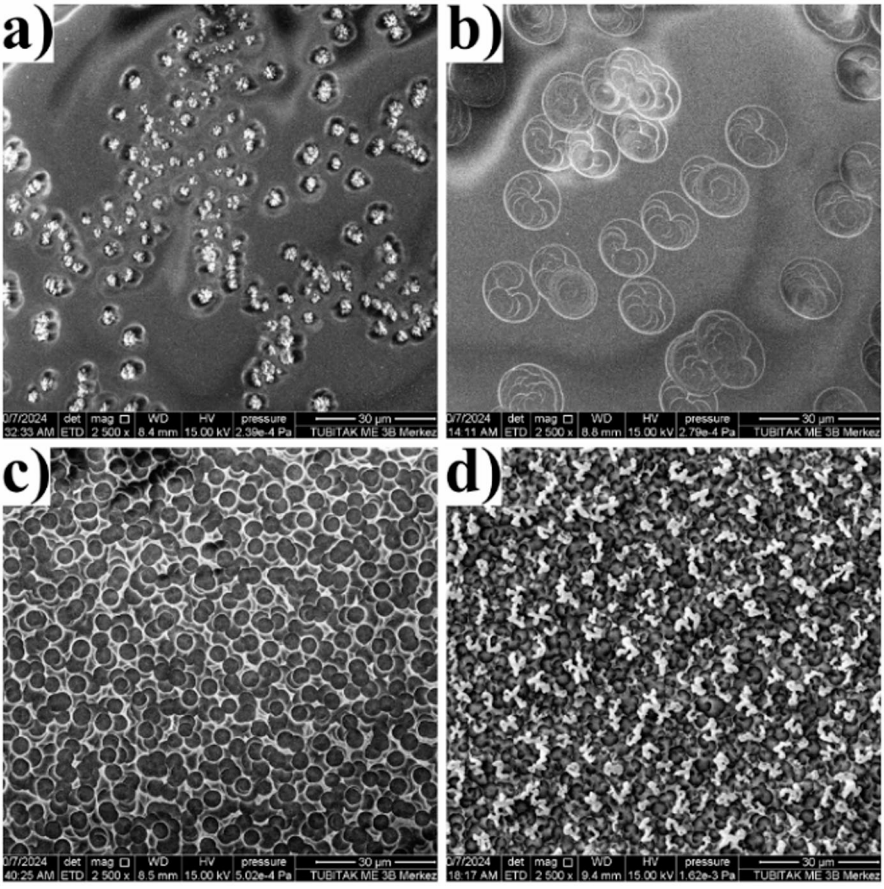

Fig. 7 SEM images of the glass surface after 60 min of etching under Recipe (**a**) A, (**b**) B, (**c**) C, (**d**) D

reaction by-products, which act as temporary micro-masks during etching. Etching was repeated with Recipe C, where only the C_4F_8 concentration was increased while the other gases were kept constant and SEM images were given in Fig. 7: c). The surface was exhibited a porous morphology with densely separated and relatively smaller crater-like feature, each accompanied by well-defined bright rim-like formations, as mentioned in the introduction, which is one of the factors responsible for PISD formation. This behavior indicates that the additional C_4F_8 enhanced the free F radicals, restoring the balance between surface passivation and etching. SEM images of the glass samples etched with Recipe D were presented, in Fig. 7: d), where the gas composition was modified by increasing C_4F_8 concentration, reducing the O_2 content, and removing both Ar and SF_6 from the mixture. Under these conditions, the etching process produced the smallest crater-like features, a nearly smooth and uniform surface without noticeable defects. The elimination of Ar suppressed sputter-effect-induced micro-masking that could lead to PISD formation. Further, with increasing C_4F_8 content, the plasma chemistry favored the generation of CF_x fragments, resulting in enhanced surface passivation. This effect was observed in the SEM image as numerous bright features surrounding the semi-circular surface morphology. Rather than indicating uncontrolled residual accumulation, these features suggest a stabilized passivation layer that locally moderates chemical etching.

The quantitative EDS analysis is given in Table 3, while the corresponding analysis regions are provided in Supplementary Information Fig. S1. These results clarified that the surface components were highly dependent on plasma compositions, correlating with the observed morphological changes under different plasma chemistries.

In addition to the substrate-related elements (Si, Na, K, and Al) originating from the glass matrix, the surface also exhibited notable amounts of fluorine (F), chlorine (Cl), and Ni, indicating the effects of plasma-induced reactions and material redeposition. The detection of Cl was attributed to residues from the chloride-based electrolyte used during the electrodeposition of the Ni hard mask as mentioned with detailed in Sect. Sample Preparation which may remain as adsorbed or entrapped salts on the surface. The persistence of Cl signals in Recipes A–C suggests incomplete removal of these chloride species, further promoted by strong sputter-effect-induced erosion, which could remain attached to the surface or embedded within redeposited particulates. Notably, F was detected in the EDS spectra of all investigated recipes (Recipe A–D). This consistent presence of F can be explained by two complementary mechanisms: (i) the use of fluorocarbon-based plasmas promotes the formation of a fluorocarbon passivation layer on the glass surface, resulting in residual fluorine even after etching; (ii) highly reactive F radicals can chemically interact with network-modifying elements, such as Na, K and Al, forming F-rich residual accumulation as

Table 3 EDS analysis of the glass surface after 60 min of etching

Element	Atomic %			
	Recipe A	Recipe B	Recipe C	Recipe D
O	49.17	36.70	25.72	27.58
Si	25.41	23.88	19.48	24.63
Na	8.01	9.43	14.55	10.33
Al	1.58	1.44	4.12	3.89
K	0.49	0.49	0.32	1.13
F	11.94	27.18	32.49	32.44
Cl	3.39	0.89	0.48	-
Ni	-	-	2.84	-

non-volatile halogens like AlF_3, NaF, and KF [8]. As a result, F-containing residues may remain bound to the surface or incorporated into redeposited material. In Recipe A, the F detected on the surface was mainly attributed to non-volatile residual species, as the plasma was composed of SF_6-driven fragments. However, the amount and/or energetic effectiveness of these fluorine species were insufficient to sustain etching. In particular, the introduction of O_2 and a small amount of C_4F_8 into the plasma significantly influenced the etching mechanism by modifying both gas-phase reactions and surface processes. Previous studies have shown that oxygen radicals scavenge carbon from gas-phase fluorocarbon (CF_x) species, promoting CO formation and releasing free F radicals [17]. Consequently, when using an O_2 containing gas mixture for etching, it is important to choose the optimal O/F ratio, which affects both the etched structure, surface composition and etching rate [18]. To generate more F radicals, O_2 and a small amount of C_4F_8 were introduced, forming Recipe B, resulting in a significant increase in F-rich residual accumulation on the surface. To further increase the F concentration, C_4F_8 content was increased, resulting in the formation of Recipe C. In this regime, F radicals contribute both formation of F-rich surface passivation and etching reaction, while energetic Ar enhance material removal through sputter-effect-induced erosion. The combined physical-chemical etching environment causes erosion of the Ni hard mask. Consistently, EDS analysis showed the presence of Ni on the surface, indicating erosion of the Ni hard mask induced by Ar-dominant sputtering. The sputtered Ni species were not efficiently removed from the plasma system and redeposited onto the surface. The detection of Ni, Cl, and F in the EDS results indicates the composition of the well-defined bright rim-like formations noted in the SEM image. To suppress excessive sputter-effect-induced erosion, Ar was removed in Recipe D, thereby reducing erosion of the Ni hard mask. In addition, the elimination of SF_6 and the increased contribution of a C_4F_8, plasma shifted the etching mechanism. Notably, Recipe D exhibited no detectable Cl or Ni signals, while maintaining a high F content. This indicates that the C_4F_8-dominant plasma enabled efficient etching performance, preventing mask degradation. Overall, the EDS results demonstrate a clear transition from Cl and Ni contaminated surfaces in Recipe A to contamination-free surfaces in Recipe D, highlighting Recipe D as the most optimized and ideal condition among the investigated plasma recipes.

The glass substrates were subjected to plasma etching under the specified process conditions, and the resulting etch depths were measured using a profilometer every 30 min after the initial 60 min of etching. The etch rates were then calculated from the ratio of etch depth to etch time (etch depth / etch time). Figure 8 presents the variation of etch rate as a function of etch time for the different plasma recipes, and the etching depths measured as a result of etching was written in the graph.

The etch behavior observed in this figure is consistent with the morphological and compositional changes identified by SEM and EDS analyses, highlighting the evolution of the plasma–surface interaction regime with changing gas chemistry. In Recipe A, the etch rate decreased markedly with time, reaching an etch depth of only 24.8 μm after 120 min. SEM images revealed island-like PISD morphology, while EDS analysis indicated the presence of Cl and F-rich residues. These findings suggest that the etching process was limited by redeposition of non-volatile species and contaminants formed during sputter-effect-induced erosion. Unlike Recipe A, where the high Ar content induced strong sputter dominant erosion accompanied by material redeposition, the addition of C_4F_8 and O_2, forming Recipe B, fundamentally altered the plasma chemistry and led to a marked suppression of the etching

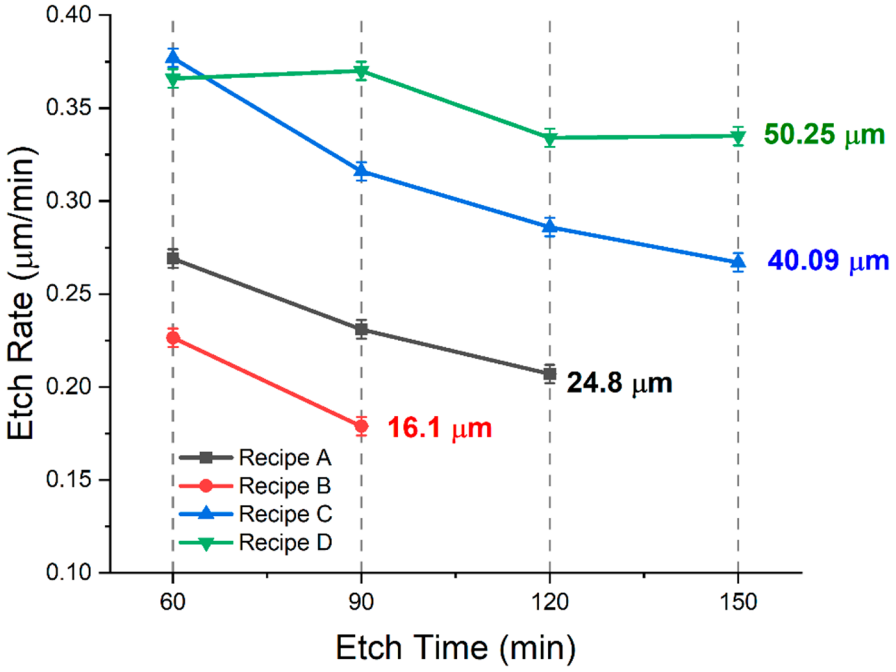

Fig. 8 Etch time versus etch depth results of all recipes

process. A moderate increase in the concentration of F radicals was not sufficient to achieve effective silicon etching or to ensure complete surface cleaning. The etch rate decreased even further, yielding an etch depth of only 16.1 μm after 90 min. This pronounced suppression of etching is attributed to enhanced F-rich accumulation, which dominated over chemical etching and effectively limited material removal. Further increasing the C_4F_8 concentration in Recipe C, reinitiated etching and increased the overall etch depth to 40.09 μm after 150 min. The simultaneous detection of Ni and Cl peaks indicates redeposition of sputtered particles resulting in a reduction of etch rate over time. In Recipe D, the etch rate was the most stable among all recipes, and after 150 min, the total etch depth reached 50.25 μm. SEM observations confirmed a smoother and more uniform surface morphology, while EDS analysis showed the absence of Cl and Ni residues. These results indicate that optimized C_4F_8/O_2 mixtures effectively suppress contamination and micro-masking, enabling a chemically controlled etching regime with improved surface quality and maximum etch depth among all recipes.

Among all investigated conditions, Recipe D demonstrated the most favorable etching performance, characterized by smooth surface, and impurity-free morphology, making the etched micropillar structures promising candidates for use in microfluidic platform applications. Finally, cross-sectional SEM image of the micropillar area on the sample that was etched for 150 min using Recipe D is presented in Fig. 9, revealing an etch depth of approximately 47.6 μm, which is in good agreement with the profilometry results shown in Fig. 8 (50.25 μm).

The etching process was carried out at a relatively high ICP power of 2000 W (Table 2) to ensure stable plasma generation and maintain sufficient plasma conditions for deep

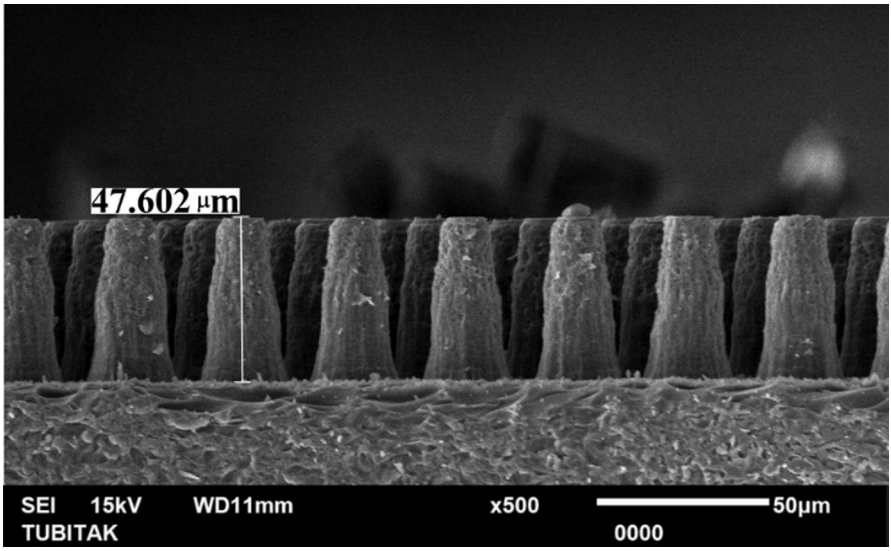

Fig. 9 Cross-sectional SEM image of etched surface with Recipe D

glass etching. Under such energetic conditions, partial erosion of the Ni hard mask was inevitable. Nevertheless, the selected gas chemistry effectively suppressed the formation of micro-masks and redeposited particles on the surface, maintaining smooth feature profiles throughout the process. The micropillar array exhibits well-defined sidewalls and a uniform height distribution, indicating efficient by-product evacuation and controlled surface passivation. However, the slight rounding and surface degradation observed near the top regions of the pillars can be attributed to localized glass impurities and partial PISD, accompanied by minor compositional variations and F-rich residues. A detailed inspection of the upper regions of the micropillars further reveals evidence of Ni hard mask erosion. This behavior is attributed to minor fluctuations in the substrate table temperature during high-power ICP operation. Despite the use of auxiliary stabilization systems, such temperature variations are difficult to fully eliminate and can locally alter reaction kinetics and residual desorption rates, contributing to the observed non-uniformities near the pillar tops. Overall, the etch rate results are consistent with the SEM and EDS analyses, confirming that uniform glass etching is achieved when plasma parameters and gas composition are optimized to balance between sputter-effect-induced erosion and chemical etching as demonstrated by Recipe D.

Optical Emission Spectroscopy Analysis

The OES spectra in Fig. 9 shows the emission lines corresponding to different gas compositions employed during ICP-RIE of borosilicate glass. These spectra were obtained under 500 W ICP power, 0 W RF bias power, and 1.33 Pa pressure. Although the etching processes were carried out at higher powers (2000 W ICP and 300 W RF bias power), the significantly increased signal magnitudes at such conditions hindered reliable detection and interpretation of the plasma recipe [19]. The spectra presented in Fig. 10 indicated that the optical activity varied significantly with the applied gas chemistry. Also, the etching regime in reci-

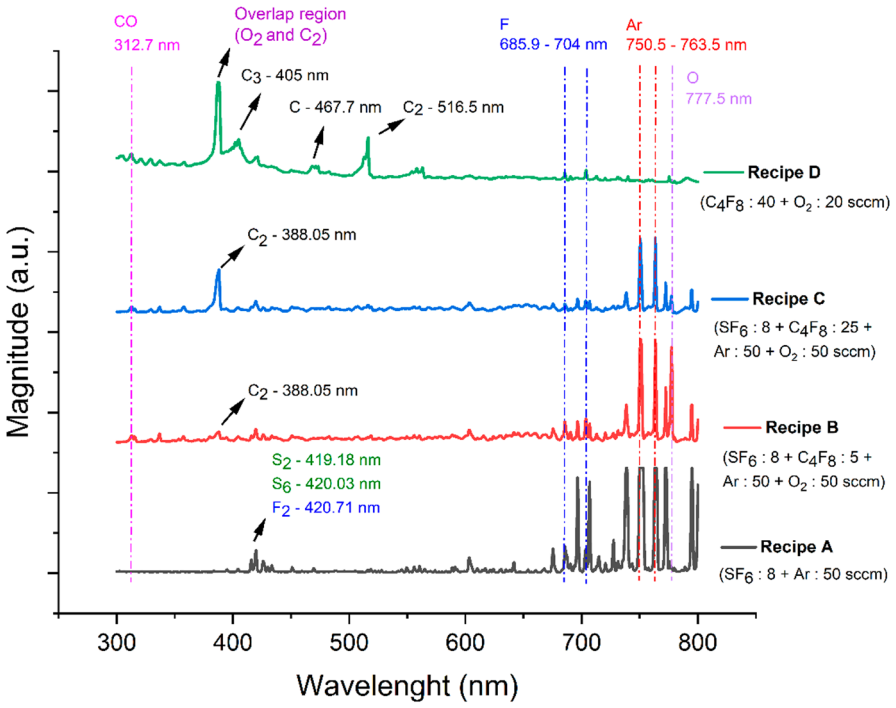

Fig. 10 OES of different gas chemistries

pes was derived not only from OES distribution ratios but also from a combined assessment of surface morphology and agglomerated regions compositional analysis.

In Recipe A, F from SF_6 enabled the formation of volatile compounds such as SiF_4 and BF_3, while Ar contributed energetic ions responsible for physical sputtering. The dissociation of SF_6 was confirmed by emission peaks observed 419–421 nm corresponding to S_2 [20] and F_2 [20]. However, the optical emission spectra were dominated by intense Ar lines at 750.5 [21] − 763.5 nm [12], whereas F-related peaks at 685.9 [12] − 704 nm [21]. This does not necessarily indicate a low chemical activity of F, as reactive F radicals are rapidly consumed at the surface and may not be efficiently detected by OES. The etching regime in Recipe A was therefore not inferred solely from the OES intensity ratios, but primarily from the surface morphology and compositional analysis. SEM images showed agglomerated surface regions and particle redeposition, indicating micro-masking effects commonly associated with sputter-effect-induced erosion conditions. This interpretation was further supported by EDS results, which showed the F-rich residues and presence of redeposited Cl species. In Recipe B, the addition of O_2 and a small amount of C_4F_8, altered the plasma chemistry. The existence of C_2 emission at 388.05 nm [20] indicates the dissociation of C_4F_8. Also, the presence of CO peak at 312.7 nm [22] confirms reactions between O and C. This behavior is consistent with the previously described O scavenging mechanism, in which O binds to C and promotes fluorine release [17, 23]. However, the dominant O emission at 777.5 nm [20] indicates that oxygen is not completely consumed by carbon and is still present in the plasma, while the reduction of etch rate and the high F-rich accumulations found in the EDS results suggest that the plasma requires more C_4F_8 to enter the etching

regime. In Recipe C, C_4F_8 was increased to further modify the plasma. The C_2 emission at 388.05 nm risen and indicates enhanced dissociation of C_4F_8, while the reduction in O emission suggests that O is largely consumed through reactions with C-containing species. The corresponding increase in etch rate implies a higher availability of F radicals, promoting chemical etching. In parallel, sputter-effect-induced erosion remains significant, as evidenced by the continued presence of Ar emission lines in the OES spectra. The coexistence of chemical and sputtering effects results in to etching of the Ni mask, and Cl-containing residues cannot be efficiently removed from the surface. Furthermore, the distinct PISD morphology observed in SEM images indicates that the etching process becomes poorly controlled under these conditions. To eliminate Ar-related micro-masking observed in Recipes A, B, and C, Ar and SF_6 were removed and the plasma consisted solely of a C_4F_8/O_2 mixture, Recipe D. The absence of Ar emission lines in the spectrum allowed clear detection of molecular bands. In the OES spectra, the presence of CO emission, together with the absence of a distinct atomic O peak, indicates that O was efficiently consumed through reactions with C-containing species. The spectral region between 385 and 390 nm can therefore be regarded as an O – C overlap region, while the strong emissions associated with C_3 (~ 405 nm), C (467.7 nm), and C_2 (516.5 nm) [20] confirm an active C-rich plasma chemistry. EDS analysis confirmed the absence of Ni and Cl contamination; nevertheless, F-rich surface accumulations occurred verifying that the C_4F_8/O_2 plasma established a balanced regime between chemical etching and material removal. This is in good agreement with the high and nearly constant etch rate, pointing to a predominantly etching regime. SEM images further support this interpretation, as no pronounced PISD structures are observed and the surface morphology remains relatively smooth. Overall, these observations indicate that Recipe D enables a stable, F-driven chemical etching process with improved surface control and minimal sputter-effect-induced erosion.

Conclusion

Systematic investigation of the optical microscopy, SEM, EDS, and OES results indicated a strong correlation between surface morphology, etching performance, and plasma composition during borosilicate glass etching. OES, together with SEM, EDS, and etch rate measurements, enabled a comprehensive evaluation of the plasma–surface interactions governing material removal and surface morphology evolution. In summary, the evolution from Recipe A to Recipe D demonstrates a clear transition from an Ar-dominated and sputter-effect-induced erosion regime toward a stable, F-driven chemical etching process. Since the excess O suppresses effective F activity, F-rich surface residues resulting in low etch rates. Increasing the C_4F_8 content enhances component dissociation and F availability, resulting in higher etch rates; however, the simultaneous presence of Ar introduces significant sputter-effect-induced erosion, causing mask erosion, residue retention, and uncontrolled surface morphology. In contrast, Recipe D eliminates both Ar and SF_6, enabling efficient O consumption by C species and stabilizing the F chemistry. This condition yields a high and nearly constant etch rate, smooth surface morphology without pronounced PISD structures, and minimal contamination, indicating that Recipe D operates within a well-controlled chemical etching regime. This framework clarifies the plasma–surface interactions providing a comprehensive basis for developing clear surfaces, contamination-free

ICP-RIE processes in future microfabrication technologies. Future studies may extend the optimized plasma conditions to the fabrication of glass-based microfluidic structures, where depth control and surface morphology are critical. A deeper understanding of plasma–surface interactions could further improve microfabrication producibility, particularly for complex channel geometries and high-aspect-ratio features. Such advances would support the broader integration of plasma-etched glass components in microfluidic and lab-on-chip applications.

Supplementary Information The online version contains supplementary material available at https://doi.org/10.1007/s11090-026-10666-4.

Acknowledgements The authors would like to thank Şirin Say and Şeyma Soykan for their assistance with sample preparation in the laboratory. The authors gratefully acknowledge the Scientific and Technological Research Council of Turkey (TUBITAK) due to the financial support for the Project 22AG030 and 120N816.

Author Contributions Authors' Contribution All authors reviewed the manuscript. All authors contributed to the discussion and gave helpful feedback. CT, IG: Experiments planning and conduction; DN, EZ: Main text preparation; DN, CT, MS: Photolithography, mask deposition, ICP-RIE process; DN, CT: SEM investigation; DN: Sample profilometry; DN: OES investigation; DN: Literature investigation, the representation of the results and feedback; CT: Head of the research group, consulting, and discussion.

Funding Open access funding provided by the Scientific and Technological Research Council of Türkiye (TÜBİTAK).

Data Availability No datasets were generated or analysed during the current study.

Declarations

Competing interests The authors declare no competing interests.

Open Access This article is licensed under a Creative Commons Attribution 4.0 International License, which permits use, sharing, adaptation, distribution and reproduction in any medium or format, as long as you give appropriate credit to the original author(s) and the source, provide a link to the Creative Commons licence, and indicate if changes were made. The images or other third party material in this article are included in the article's Creative Commons licence, unless indicated otherwise in a credit line to the material. If material is not included in the article's Creative Commons licence and your intended use is not permitted by statutory regulation or exceeds the permitted use, you will need to obtain permission directly from the copyright holder. To view a copy of this licence, visit http://creativecommons.org/licenses/by/4.0/.

References

1. Davis JA, Inglis DW, Morton KJ, Lawrence DA, Huang LR, Chou SY, Sturm JC, Austin RH (2006) Deterministic hydrodynamics: Taking blood apart. Proc Natl Acad Sci 103:14779–14784. https://doi.org/10.1073/pnas.0605967103
2. Choi SS, Kim D, Park MJ (2004) Fabrication of Double Aperture for Nearfield Optical Trapping. J Korean Phys Soc 45:1500–1504
3. Yu X, Ye Y, Zhu P, Wu L, Shen R, Zhu C (2025) Wet Anisotropic Etching Characteristics of Si{111} in KOH-Based Solution. ACS Omega 10:2940–2948. https://doi.org/10.1021/acsomega.4c09272
4. Weigel C, Brokmann U, Hofmann M, Behrens A, Rädlein E, Hoffmann M, Strehle S, Sinzinger S (2021) Perspectives of reactive ion etching of silicate glasses for optical microsystems. J Opt. https://doi.org/10.1117/1.JOM.1.4.040901. Microsyst;1

5. Osipov AA, Fumina AE, Speshilova AB, Endiiarova EV, Osipov AA, Alexandrov SE (2024) Optical emission spectroscopy as a method for evaluating the change in Si etching structures profile in ICP SF6/C4F8 plasma: Microstructures. J Vac Sci Technol A 42:063001. https://doi.org/10.1116/6.0003809
6. Goyal A, Hood V, Tadigadapa S (2006) High speed anisotropic etching of Pyrex® for microsystems applications. J Non-Cryst Solids 352:657–663. https://doi.org/10.1016/j.jnoncrysol.2005.11.063
7. Li X, Ling L, Hua X, Fukasawa M, Oehrlein GS, Barela M, Anderson HM (2003) Effects of Ar and O2 additives on SiO2 etching in C4F8-based plasmas. J Vac Sci Technol Vac Surf Films 21:284–293. https://doi.org/10.1116/1.1531140
8. Park JH, Lee N-E, Lee J, Park JS, Park HD (2005) Deep dry etching of borosilicate glass using SF6 and SF6/Ar inductively coupled plasmas. Microelectron Eng 82:119–128. https://doi.org/10.1016/j.mee.2005.07.006
9. Leech PW (1999) Reactive ion etching of quartz and silica-based glasses in CF4/CHF3 plasmas. Vacuum 55:191–196. https://doi.org/10.1016/S0042-207X(99)00146-3
10. Li X, Abe T, Esashi M (2001) Deep reactive ion etching of Pyrex glass using SF6 plasma. Sens Actuators Phys 87:139–145. https://doi.org/10.1016/S0924-4247(00)00482-9
11. Choi DY, Lee JH, Kim DS, Jung ST (2004) Formation of plasma induced surface damage in silica glass etching for optical waveguides. J Appl Phys 95:8400–8407. https://doi.org/10.1063/1.1739525
12. Hong SJ, Park JS, Seo DS, Kim HW (2009) Statistical Analysis of Emission Intensity for Silicon Dioxide Etching Using Optical Emission Spectroscopy Data. J Korean Phys Soc 55:1873–1876. https://doi.org/10.3938/jkps.55.1873
13. Salafi T, Zhang Y, Zhang Y (2019) A Review on Deterministic Lateral Displacement for Particle Separation and Detection. Nano-Micro Lett 11:77. https://doi.org/10.1007/s40820-019-0308-7
14. Boukhouete A, Boumendjel S, Sobhi N-E-H (2021) Effect of current density on the microstructure and morphology of the electrodeposited nickel coatings. Turk J Chem 45:1599–1608. https://doi.org/10.3906/kim-2102-46
15. Bogaerts A (1995) Modeling of metastable argon atoms in a direct-current glow discharge. Phys Rev A 52:3743–3751. https://doi.org/10.1103/PhysRevA.52.3743
16. Dorranian D, Alizadeh M (2014) Effect of negative oxygen ions on the characteristics of plasma in a cylindrical DC discharge. J Theor Appl Phys 8:122. https://doi.org/10.1007/s40094-014-0122-z
17. Donnelly VM, Kornblit A (2013) Plasma etching: Yesterday, today, and tomorrow. J Vac Sci Technol Vac Surf Films 31:050825. https://doi.org/10.1116/1.4819316
18. Osipov AA, Iankevich GA, Speshilova AB, Gagaeva AE, Osipov AA, Enns YB, Kazakin AN, Endiiarova EV, Belyanov IA, Ivanov VI, Alexandrov SE (2022) OES diagnostics as a universal technique to control the Si etching structures profile in ICP. Sci Rep 12:5287. https://doi.org/10.1038/s41598-022-09266-x
19. Kim DH, Choi JE, Hong SJ (2021) Analysis of optical emission spectroscopy data during silicon etching in SF_6 /O_2 /Ar plasma. Plasma Sci Technol 23:125501. https://doi.org/10.1088/2058-6272/ac24f4
20. Kramida A, Ralchenko Y (1999) NIST At Spectra Database NIST Standard Reference Database 78. https://doi.org/10.18434/T4W30F
21. Bates RL, Stephan Thamban PL, Goeckner MJ, Overzet LJ (2014) Silicon etch using SF6/C4F8/Ar gas mixtures. J Vac Sci Technol Vac Surf Films 32:041302. https://doi.org/10.1116/1.4880800
22. Krstulović N, Labazan I, Milošević S, Cvelbar U, Vesel A, Mozetič M (2006) Optical emission spectroscopy characterization of oxygen plasma during treatment of a PET foil. J Phys Appl Phys 39:3799. https://doi.org/10.1088/0022-3727/39/17/014
23. Butterbaugh JW, Gray DC, Sawin HH (1991) Plasma–surface interactions in fluorocarbon etching of silicon dioxide. J Vac Sci Technol B Microelectron Nanometer Struct Process Meas Phenom 9:1461–1470. https://doi.org/10.1116/1.585451

Publisher's Note Springer Nature remains neutral with regard to jurisdictional claims in published maps and institutional affiliations.

Authors and Affiliations

Duygu Nuhoğlu[1,2] · Meryem Sarigüzel[2] · Cihat Taşaltın[2] · Ilke Gurol[2] · Esra Zayim[1]

✉ Duygu Nuhoğlu
kalkandu@itu.edu.tr; duygu.nuhoglu_d@tubitak.gov.tr

Meryem Sarigüzel
meryem.sariguzel@tubitak.gov.tr

Cihat Taşaltın
cihat.tasaltin@tubitak.gov.tr

Ilke Gurol
ilke.gurol@tubitak.gov.tr

Esra Zayim
ozesra@itu.edu.tr

[1] Department of Physics Engineering, Istanbul Technical University, Istanbul 34469, Maslak, Turkey

[2] Marmara Research Center, TUBITAK, Materials Technologies, P.O. Box 21, Gebze- Kocaeli 41470, Turkey